SCIENTIFIC REPORTS

OPEN

SUBJECT AREAS:
COLLOIDS
ENGINEERING

Received
11 July 2013

Accepted
4 February 2014

Published
4 March 2014

Correspondence and requests for materials should be addressed to A.M. (marmur@technion.ac.il)

Rate of Bubble Coalescence following Quasi-Static Approach: Screening and Neutralization of the Electric Double Layer

Yael Katsir & Abraham Marmur

Department of chemical engineering, Technion – Israel Institute of Technology, Haifa 32000, Israel.

Air-bubble coalescence in aqueous electrolytic solutions, following quasi-static approach, was studied in order to understand its slow rate in purified water and high rate in electrolytic solutions. The former is found to be due to surface charges, originating from the speciation of dissolved CO_2, which sustain the electric double layer repulsion. Rapid coalescence in electrolytic solutions is shown to occur via two different mechanisms: (1) neutralization of the carbonaceous, charged species by acids; or (2) screening of the repulsive charge effects by salts and bases. The results do not indicate any ion specificity. They can be explained within the DLVO theory for the van der Waals and electric double layer interactions between particles, in contrast to observations of coalescence following dynamic approach. The present conclusions should serve as a reference point to understanding the dynamic behavior.

Air-bubble coalescence is frequently encountered in nature as well as in industry[1–37]. In some cases, rapid coalescence is preferred, e.g. to avoid clogging of a system. In others, a relative slow coalescence is required, in order, for example, to keep the total interfacial area of the bubbles as high as possible. An example of a natural process is the formation of bubbles during breaking of seawater waves. This foam stays stable for a short time, during which the bubbles enhance the dissolution of oxygen and other weakly soluble gases[7,8]. Eventually, the coalescence of the bubbles with the sea-air interface leads to transfer of gas and ionic aerosols to the atmosphere[5–7]. Industrial examples include mass transfer processes in bubble columns, distillation towers, gas-liquid contactors, bioreactors, electrochemical cells etc.[8,9].

Relatively slow bubble coalescence (seconds or minutes) in aqueous solutions containing certain concentrations of electrolytes, was apparently first observed in 1929[10]. This phenomenon has been widely discussed[10–37], since it appears to be in qualitative contradiction to the DLVO (Derjaguin, Landau, Verwey, and Overbeek) theory[38], which describes the stability of colloidal particles in a medium, by calculating the combined effects of van der Waals (vdW) attraction and electric double layer (EDL) repulsion between the particles. It predicts accelerated bubble coalescence in aqueous solutions of electrolytes compared with purified water. So far, only partial explanations of this apparent contradiction have been given, based on surface elasticity[2,15,17,39,40], surface diffusion[41], ion partitioning at the tested liquid-air interface[37,42,43] hydration and structural forces[26,44,45], effective/partial immobilization of interfaces, and deformation effects[46–49].

Various electrolytes have been investigated over the years, using a variety of methods to study bubble coalescence behavior. Since bubble coalescence is actually a process of thin film rupture, it has been studied by methods that apply to either whole bubbles or isolated thin films: a bubble column[11–20], pairs of bubbles[12,19,21–26], bubbles rising to the interface[27–30], a liquid thin-film between two gas-phases[31–33], and two bubbles in Atomic Force Microscopy (AFM)[34–36]. These studies have revealed the effect of electrolyte type and concentration on the rate of bubble coalescence, mostly when the approach of the coalescing bubbles is dynamic (approach velocity higher than 10 μm/sec). The transition between rapid coalescence (order of magnitude of milliseconds or seconds) and relatively slow coalescence occurs only with certain electrolytes and at specific concentrations (termed "transition concentrations"[14]).

Craig *et al.*, using the bubble column method, empirically classified the ions of the electrolytes as type α or β. They found that αα and ββ electrolytes in aqueous solutions slow bubble coalescence, while αβ and βα electrolytes have no meaningful effect compared with purified water[14]. This classification was supported also by the results

obtained using the thin-film method[31]. They later extended the classification to include mixed aqueous electrolytes, using the same experimental technique[15]. There are very few exceptions to the "α, β" classification: slow coalescence was observed also for αβ and βα electrolytes, but at higher transition concentrations[21]. Unfortunately, in other studies, only αα electrolytes were used, hence the ion specificity phenomenon needs to be further studied.

Recently, the approach velocity between the two interfaces, using the thin-film method, was found to be a key issue for the coalescence behavior in aqueous solutions of electrolytes[32]. For dynamic approach (velocities above 150 μm/sec), the observations supported previous studies. But, for quasi-static approach (below 1 μm/sec), the observations were completely different: slow coalescence in purified water (minutes to hours) and rapid coalescence for electrolyte solutions (seconds). For intermediate approach velocities(between 1 and 150 μm/sec) transient films were observed.

In contrast to the dynamic-approach case, recent observations for quasi-static approach (velocities below 1 μm/sec) show behavior that may be in qualitative agreement with the DLVO theory. Yaminsky et al.[32] studied the coalescence of purified-water films and aqueous NaCl solutions films, and demonstrated some agreement with the DLVO theory by fitting the disjoining-pressure isotherm to experimental data. A later study by Tabor et al.[34], which also explored coalescence under quasi-static approach (<0.2 μm/sec), demonstrated that bubble coalescence in water is highly dependent on gas type and pH. Their results with air bubbles in "as is" purified water (pH = 5.8) are in contradiction with those of Yaminsky et al.[32], since the latter demonstrated a stable film of purified water for pH = 5.8, while Tabor et al. claimed it is not stable under these conditions. This contradiction is associated with the fundamental question regarding the origin of the double layer charge. Yaminsky et al.[32] attributed the surface charge that keeps the film stable to hydroxyl ions, following previous literature. Tabor et al.[34], on the other hand, discussed the possibility of the charge originating from CO_2 speciation in water, mainly with regard to CO_2 bubbles.

Thus, three main questions regarding air bubble coalescence behavior seem yet to be open: (a) can it be explained by the DLVO theory following quasi-static approach, and what makes it so different following dynamic approach? (b) if it can be explained by the DLVO theory, what is the origin of the surface charge that keeps the thin film stable? (c) what is the origin of specificity of the effect of various electrolytes, and how is it affected by the approach velocity? The objective of the present paper is to explain quasi-static bubble coalescence behavior by answering those of the above questions that relate to quasi-static approach in purified water and various electrolytic solutions. The experimental method chosen was a bubble growing towards the tested liquid-air interface. The reasons for this choice were: (a) it allows simple optical visualization of the coalescence process at the required accuracy level; (b) it enables limitation of the bubble approach velocity to sufficiently low values; and (c) it has features that are similar to both bubble column and thin film systems.

Results

Air-bubble coalescence was studied using the system shown in figure 1a. A single bubble was produced by pushing air from a syringe through a capillary tube, submerged in the tested liquid (to be referred to simply as "the liquid"), with the aid of a micrometer. The liquid-air interface plays the role of the second (very large) bubble, with which the formed bubble coalesces. The process was recorded with the aid of a microscope-video set (magnification of about ×20). The bubble was reflected by the liquid-air interface, and this reflection enabled a rough estimation of the distance between them (figure 1b). The bubble was slowly grown until the film thickness between the bubble and liquid-air interface was about 100 μm. From this point on, the bubble continued to slowly expand towards the liquid-air interface, due to a slight pressure difference that remains or arises in the syringe, probably because of relaxation motion of the piston. The measured approach velocity of the bubble was within the range of 1–10 μm/sec. Then, the bubble reached close contact with the liquid-air interface, and finally they coalesced.

The rate of coalescence is represented by the coalescence time, which is defined as the time difference between the moment at which the top of the bubble is observed to contact its reflection and the last frame before coalescence (see figure 2). Emphasis was put on the transition between two extreme coalescence behaviors. One extreme is rapid coalescence (time of about 1–10 sec.) or very rapid coalescence (less than 0.06 sec., which is the time interval between two video frames); no visible deformation of the bubble interface could be observed during these rapid coalescence processes, and high reproducibility of coalescence times was observed as can be seen by the low standard deviations (figure 3). The other extreme is slow coalescence, characterized by long coalescence times of 15 minutes or more (even hours), while the bubble is being deformed at its top (figure 2, the last frame before coalescence). The uncertainty in the long coalescence times is mostly due to the identification of the moment of contact, since the final coalescence stage lasts less than ~0.06 second (two frames). This uncertainty was found to be limited to less than ten frames, thus the coalescence time resolution in these experiments was about 1 second (for more details, see methods). Since the difference between long and short coalescence times is at least two orders of magnitude, this resolution for slow coalescence is more than adequate for the present purposes.

Figure 3 presents the measured coalescence times vs. calculated ionic strengths of tested liquids. Coalescence times longer than 15 min. are indicated by small upward arrows located at the 15 min. level. The ionic strength was chosen as the independent variable because it is a determining factor in double layer interactions. It was calculated for each tested liquid, according to the following equation

$$I = 0.5 \sum C_i z_i^2 \qquad (1)$$

where z_i is the valence of ion i, and C_i is its molar concentration. In addition to the equilibrated concentration of the ions derived from the electrolyte, we considered the carbonaceous ions resulting from the equilibrium of CO_2 dissolved in water (HCO_3^-, CO_3^{2-}, H_2CO_3), and self-ionization of water. The results of these calculations are shown in figure 4, in terms of the ratio between the carbon species as a function of pH[34,50]. Purified water, exposed to air under standard conditions, has slightly acidic pH (5.8) due to dissolved CO_2 and its equilibrated species.

As shown in figure 3, the coalescence time in purified water was longer than 15 min. In electrolyte solutions, there is a clear transition, of at least two orders of magnitude, from long coalescence times to short coalescence times within a relatively narrow range of ionic strengths. The transition ionic strength (TIS) is defined here, for simplicity, as the average between the highest ionic strength that sustains slow coalescence and the lowest ionic strength that causes rapid coalescence (see lines in figure 3 that connect these pairs of points). Table 1 lists the TIS values measured in the present work. It is clear that the TIS values of the strong acids are the lowest, with the weak acid having almost one order of magnitude higher value, probably due to its equilibrated neutral molecules in water. It is important to note that the differences in the TIS values between strong acids and salts are of orders of magnitude, way above any experimental error (see figure 3a and 3b). The TIS of the strong base is slightly higher compared with that of the salts (figure 3c). But, the weak base has aTIS similar to that of the weak acid. Again, it is probably due to its equilibrated neutral molecules in water. The above observations relate rapid or very rapid coalescence and slow coalescence to ionic strength and pH. As will be discussed below, the observed quasi-static behavior can be readily explained by employing the DLVO theory.

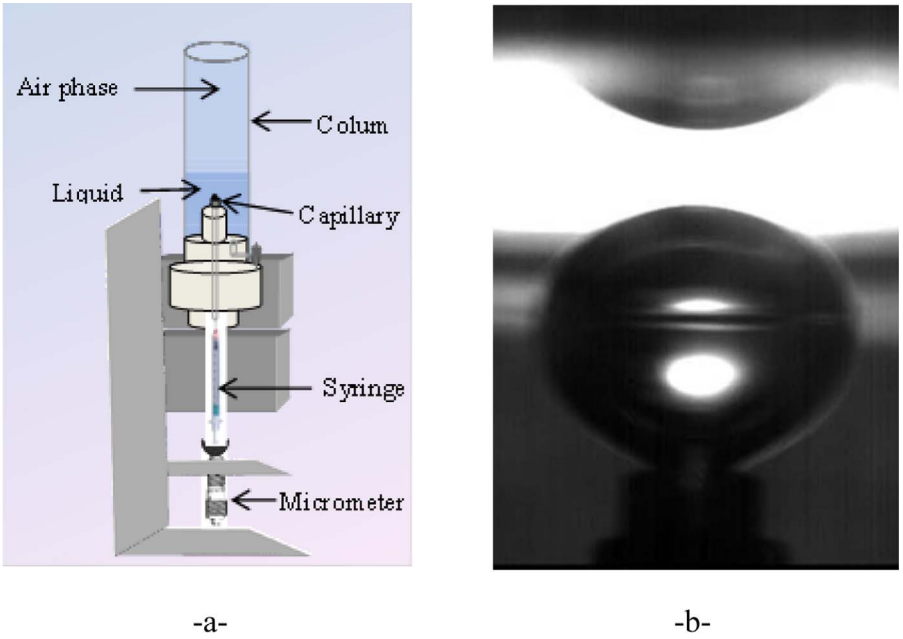

Figure 1 | Experimental system. (a) experimental set-up: Micrometer in order to push the syringe piston; Capillary (inner diameter of 0.8 mm; external diameter of 1.09 mm) attached to the syringe for forming a single bubble in the liquid; A cylindrical Perspex column contains tested liquid till 2.65 mm above the capillary. The process was followed by taking a video movie (17.4 frames/sec), which was recorded with the aid of a microscope-video set (magnification of about ×20). (b) a picture of a bubble during the stage of growing toward the liquid-air interface and reflected by it.

In order to further support such a conclusion, there is a need to find out the source of the surface charges. To demonstrate the crucial role of the carbonaceous species in forming the EDLs on the interfaces, we measured also bubble coalescence in purified water, containing negligible concentrations of carbonaceous species. For this purpose, ultra-zero air (RIVOIRA, $CO_2 < 1$ ppm) was used for blowing the bubbles as well as for the gas phase, and the reverse-osmosis water was boiled to release the dissolved carbon dioxide (since the solubility of CO_2 decreases with temperature)[51]. Indeed, the pH of the boiled purified water was 6.5, corresponding to negligible CO_2-speciation in the water (for more details, see methods). In contrast to the long coalescence times observed in the case of "as is" purified water, this "CO_2-free" system showed only rapid coalescence (3.0 ± 2.5 sec). This cannot be due to the pH increase (from 5.8 to 6.5), because when we increase the pH with a base solution, rapid coalescence occurs only at pH of about 11. The "CO_2-free" experiment was repeated 10 times and gave reproducible results (for more details, see methods). Thus, it is qualitatively shown, using a simple, straightforward way, that the EDL repulsion must be due to the presence of CO_2 in air and consequently in the water.

Discussion

The natural tendency of bubbles is to coalesce, in order to reduce their surface energy. The mutual attraction of the interfaces of the bubbles and their coalescence derive from the universal vdW interaction between the molecules at the two sides of the interfaces. Slowness of coalescence for meaningful (finite) time periods requires repulsion that opposes the vdW attraction. The DLVO theory considers repulsion in electrolytic systems, which is due to electrostatic interaction between electric double layers on the two interfaces. These are formed following preferential adsorption of ions to the surfaces. The current experimental results support the hypothesis that the phenomena associated with bubble coalescence under quasi-static conditions can be explained by the DLVO theory[32]. This conclusion may serve as a reference point for better understanding of coalescence following dynamic approach, which does not comply with the DLVO theory.

The slowness of coalescence of air bubbles in purified water indicates that there must be a repulsion force between the air-water film interfaces. Previously reported zeta-potential measurements indeed indicated that the air-water interface is (negatively) charged, with a

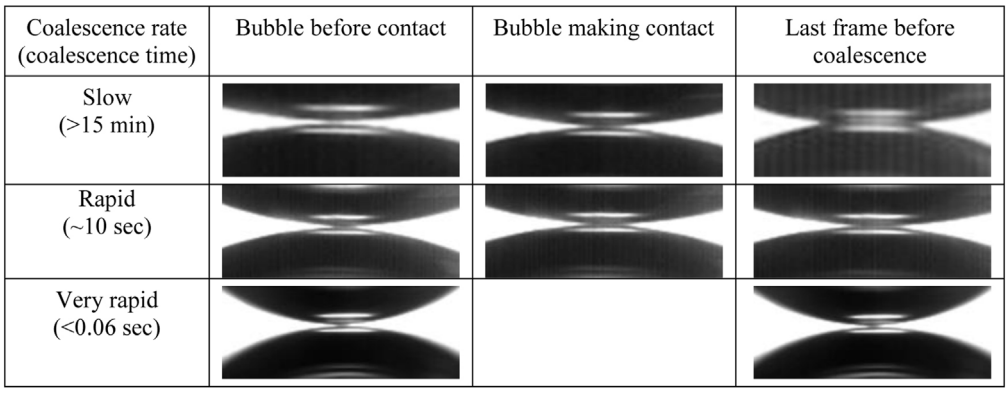

Figure 2 | Stages in the bubble coalescence process that are used for determining the coalescence time in the cases of slow, rapid, and very rapid coalescence.

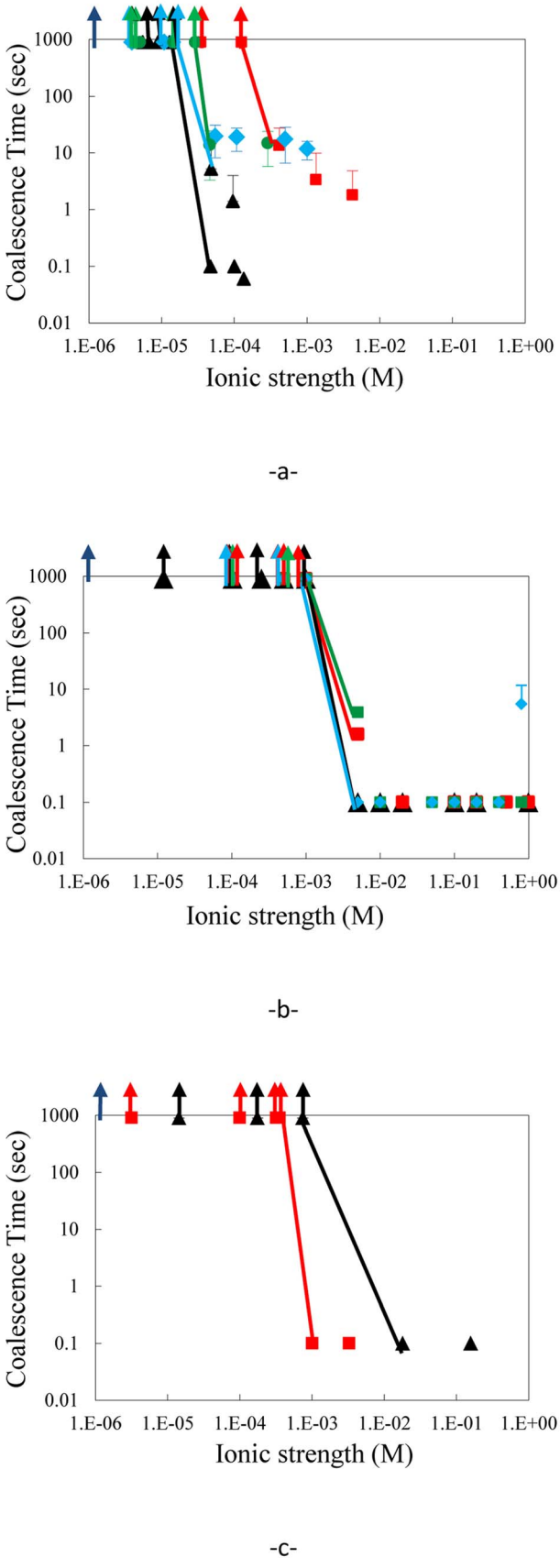

Figure 3 | Coalescence times vs. ionic strength for the various electrolytic aqueous solutions. (a) Acidic aqueous solutions. Black triangles - HCl (βα); pale-blue diamonds - HNO_3 (βα); green circles - H_2SO_4 (βα); red squares - HAc (ββ). (b) Salts aqueous solutions. Black triangles - NaCl (αα); red squares - KCl (αα); Pale-blue diamonds - KAc (αβ); green squares - NaAc (αβ). (c) basic aqueous solutions. Black triangles - NaOH (αα); red squares - NH_4OH (αα). Lines connect the highest ionic strength that sustains slow coalescence and the lowest ionic strength that causes rapid or very rapid coalescence; their average value is defined as the TIS. All long coalescence times (>15 min.) are presented as upward arrows starting from the 15 min. line. The "as is" purified water (pH = 5.8; ionic strength of 2.1×10^{-6} M), without added electrolytes, is represented, for comparison, in each figure as a blue arrow.

potential of about −40 to −60 mV[34,52–55], although the extent of the ions affinity to the air-water interface is still under debate[56–58]. The only CO_2-derived species that exists at a meaningful concentration in "as is" purified water (pH = 5.8) is HCO_3^- (see figure 4); also, the solubility of CO_2 in water at atmospheric pressure and room temperature is order of magnitude of 10^{-6} M. Therefore, the molar concentration of HCO_3^- is about two orders of magnitude higher the the concentration of OH^- at pH = 5.8. Hence, it is reasonable to associate the formation of the EDL with the dissolved CO_2. The above-mentioned experiment that showed rapid coalescence in the absence of CO_2 strongly supports this assumption. Moreover, this indicates that the carbonaceous species must be the prime source of the surface charge.Thus, it is justified, on experimental as well as theoretical grounds, to associate the formation of the EDL with the dissolved atmospheric CO_2, as Yaminsky et al.[32] suggested. Next, the coalescence results are quantitatively discussed within the framework of the DLVO theory, in order to further support the above assumption.

To facilitate the discussion, the total interaction energy between the interfaces vs. film thickness is presented in Fig. 5, for various aqueous solutions that represent those experimentally studied in this work. These energy profiles present energy-barriers that need to be overcome in order for the bubbles to coalesce. They strongly depend, as is well known, on the type and composition of the solution. The effect of an energy barrier on bubble coalescence depends mostly on two factors: the height of the barrier and the film thickness associated with the maximum in energy. If the energy barrier is too low, the thinning of the film cannot be stopped and the bubbles must coalesce. When the energy barrier is sufficiently high to retard thinning of the film, then two possible scenarios exist: (a) if the film is sufficiently thick (roughly above about 40 nm) when the energy is maximal, coalescence will be slow[31,32]; and (b) if the film is too thin at its maximum energy, thickness instabilities cause instant rupture of the film[31,32].

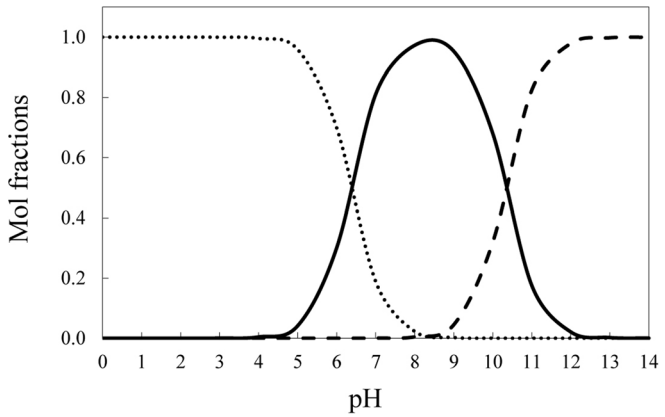

Figure 4 | Calculated concentration of carbonaceous species vs. pH. Partial pressure of CO_2 in the atmosphere is assumed constant, and acid/base are added to adjust the pH. Solid line – HCO_3^- (aq); Dashed line - CO_3^{2-} (aq); Dotted line - H_2CO_3 (aq).

Table 1 | Transition properties of aqueous electrolytesolutions: transition ionic strength (TIS), transition nominal concentration (TNC), transition pH (TpH), and transition Debye length (TDLe). TIS, TNC, and TPH are calculated as averagesbetween the values corresponding to the two extreme coalescence situations: long inhibition and rapid coalescence (as indicated by the lines in figure 2). TDLeis calculated from equation (1), using the corresponding TIS values

	Electrolyte	α,β classification by Craig et.al[14]	TIS (M)	TpH	TNC (M)	TDLe (nm)
Acids	HCl	βα	$3.0*10^{-5}$	4.6	30×10^{-5}	56
	H_2SO_4	βα	$3.7*10^{-5}$	4.3	3.9×10^{-5}	50
	HNO_3	βα	$3.4*10^{-5}$	4.5	3.0×10^{-5}	52
	HAc	αβ	$3.1*10^{-4}$	3.7	5.0×10^{-3}	17
Salts	NaCl, KCl	αα	$3.0*10^{-3}$	5.7	3.0×10^{-3}	6
	NaAc, KAc	αβ	$3.0*10^{-3}$	6.9	$3.0*10^{-3}$	6
Bases	NH_4OH	αα	$6.6*10^{-4}$	10.9	$2.8*10^{-2}$	12
	NaOH	αα	$9.4*10^{-3}$	11.4	$7.5*10^{-4}$	3

Figure 5 is based on the following equation for the total energy of interaction per unit area between two planar interfaces[59] (since the bubble size is much bigger than the thickness of the film)

$$E = -\frac{A}{12\pi d^2} + \frac{\varepsilon\chi\psi^2}{4\pi}\left[(1 - coth2\chi d) + \frac{1}{sinh2\chi d}\right] \quad (2)$$

$$A = A_{11} + A_{22} - 2\sqrt{A_{11}A_{22}} = A_{11} \quad (3)$$

The first expression on the right-hand side of eq. (2) is the vdW attraction energy, where d is the thickness of the fluid film between the bubble and liquid-air interface, and A is the Hamaker constant. In order to calculate the appropriate A for our system, namely for two bodies of the same material immersed in a different medium, we use eq. 3[60], where A_{11} and A_{22} are the Hamaker constants of water and air, respectively. This equation accounts for all possible pairwise interactions, and since the Hamaker constant of air is practically zero, the Hamaker constant of two bubbles in water turns out to be equal to that of water in vacuum ($A = A_{11} = 3.7*10^{-20}$ J). The second expression on the right-hand side of eq. 2 is the electrostatic repulsion energy, where ε is the permittivity of water, and ψ is the surface potential of both interfaces, assuming a pH-dependent potential that is, however, independent of d[34,52–55]. The Debye length, χ^{-1}, is given by

$$\chi^{-1} \equiv \sqrt{\frac{\kappa\varepsilon_0 k_B T}{2{\cdot}10^3 e^2 N_A I}} \quad (4)$$

where κ is the dielectric constant of the solution, ε_0 is the free space permittivity, k_B is the Boltzmann constant, T is the absolute temperature, e is the elementary charge, and N_A is the Avogadro number. For aqueous solutions, at room temperature, the Debye length can be calculated (in nanometers) from

$$\chi^{-1}_{(nm)} \equiv \frac{0.304}{\sqrt{I_{(M)}}} \quad (5)$$

The properties of the solutions at their corresponding TIS values, which are required for the discussion based on eqs. (2)–(5), are also shown in table 1. They are calculated by taking the average between the corresponding properties of the two solutions that were used to calculate the TIS. The latter is also used to calculate the transition Debye length (TDL).

Figure 5 shows that the experimental results may indeed be explained by the DLVO theory. The competition between vdW energy and the electrostatic repulsion energy leads to meaningful energy barriers in the cases of "as is" purified water (pH = 5.8; χ^{-1} = 211 nm; $\psi = -40$ mV), and weakly acidic solution (pH = 5.0; χ^{-1}

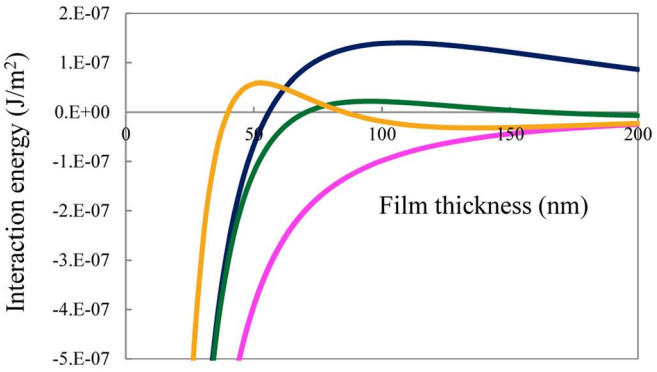

-a-

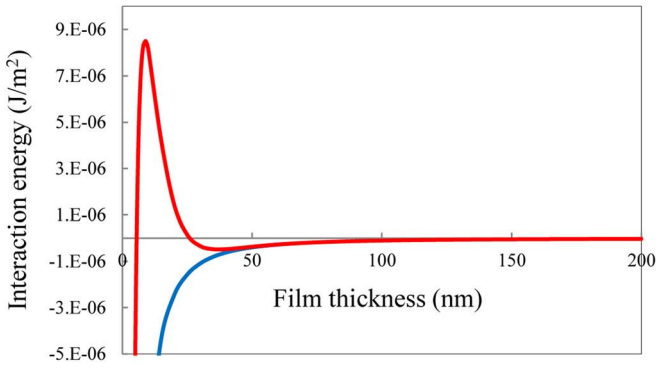

-b-

Figure 5 | Calculated interaction energy (equations 2–4) vs. film thickness for cases that resemble those studied experimentally. The surface potential (ψ) depends on the pH[34] and Debye length (calculated from the relevant ionic strength). (a) Comparison of acidic solutions. Blue line – water – pH = 5.8, $\psi = -40$ mV, χ^{-1} = 211 nm; Green line – acidic solution – pH = 5.0, $\psi = -30$ mV, χ^{-1} = 100 nm; Orange line – salt solution – pH = 5.7, $\psi = -40$ mV, χ^{-1} = 54 nm–;Pink line fits to three transition solutions: transition strong acidic solution – pH = 4.5, $\psi = -5$ mV, χ^{-1} = 54 nm; transition weak acidic solution – pH = 3.7, $\psi = 5$ mV, χ^{-1} = 17 nm; transition salt solution – pH = 5.8, $\psi = -40$ mV, χ^{-1} = 6 nm. (b) Comparison of basic solutions. Pale blue line – transition strong basic solution – pH = 11.4, $\psi = -120$ mV, χ^{-1} = 3 nm; Red line – transition weak basic solution – pH = 10.9, $\psi = -100$ mV, χ^{-1} = 12 nm.

= 100 nm; $\psi = -30$ mV), thus explaining slow coalescence and stable films at film thickness around 100 nm[31,32] (see figure 5a). The energy barrier becomes smaller with decreasing pH, till no barrier exists at pH = 4.5; $\chi^{-1} = 54$ nm; $\psi = -5$ mV, and rapid coalescence is observed. Consideration of fig. 4 leads to the conclusion that the lack of repulsion in this case stems from the lack of negatively charged, carbonaceous ions due to the low pH. Thus, one mechanism for rapid coalescence is the neutralization of the EDL by eliminating the source of the charge.

The salts hardly affect the pH, therefore their contribution is mainly to decrease the Debye length. In contrast to the transition acidic solution, salt solution at the same Debye length (pH = 5.7; $\chi^{-1} = 54$ nm; $\psi = -40$ mV) leads to meaningful energy barrier that explain slow coalescence and stable film at film thickness around 50 nm[31,32] (as can be seen in fig. 5a and eq. 2). Therefore, additional mechanism for rapid coalescence is considered for salt solutions. At the transition salts solutions (pH = 5.8; $\chi^{-1} = 6$ nm; $\psi = -40$ mV) the repulsion energy decreases sufficiently to annul the EDL repulsion. Consequently, the coalescence process is rapid, since it is dominated by the vdW attraction energy, with practically no energy barrier. Thus, the effect of salts is due to screening of the surface charges simply by increasing the electrolyte concentration (hence, Debye length decreases sufficiently). The effect of bases is similar to that of the salts; screening of surface charges that leads to rapid coalescence. As seen in figure 5b, the repulsion energy decreases sufficiently to annul the EDL repulsion when the Debye length decreases to 3 nm (transition strong base solution). We get unique energy profile for transition weak base solution, as surface potential increases with pH and Debye length decreases with the ionic strength involved, (see figure 5b and equation 2). Minimum interaction energy (attraction) occurred around 30 nm, and energy barrier (repulsion) occurred around 10 nm. As attraction energy at film thickness within the range of 30–50 nm causes instant rupture of the film[31,32], irreversible bubble coalescence was observed. Hence, energy barrier at film thickness thinner than 30 nm is not relevant with regard to soft matter, e.g bubbles.

To conclude, air-bubble coalescence following quasi-static approach was found to qualitatively and quantitatively obey the DLVO theory. In contrast to the case of dynamic approach, long coalescence times (up to hours) were observed for air bubbles in 'as is' purified-water, in agreement with the results of Yaminsky et al.[32]. The significant effect of CO_2 on air-bubble coalescence behavior is shown qualitatively (by demonstrating rapid coalescence induced by releasing the CO_2 from the water), and quantitatively (by discussing the height of the interaction energy barrier). CO_2 speciation appears to be the main source of the surface charge that keeps the purified-water film stable, since at the pH of 'as is' purified-water (pH = 5.8) the concentration of HCO_3^- (see figure 4)is about $3*10^{-6}$ M compared with that of OH^- that is only $6*10^{-9}$ M. Coalescence can be made rapid by two different mechanisms: either neutralizing the carbonaceous charge carriers (using acids), or screening the repulsive charge effects (reducing the Debye length using any electrolyte). The present observations clearly demonstrate these mechanisms. In addition, the very similar behavior in solutions of salts and bases of different "α,β" classification implies that there is no ion-specificity in coalescence phenomena following quasi-static approach.

Methods

Bubble coalescence was studied using the system shown in figure 1a. The process was followed by taking a video movie (17.4 frames/sec), which was recorded with the aid of a microscope-video set (magnification of about ×20). A single bubble was produced by pushing air from a syringe through a metal, high-quality, rounded-tip capillary tube with an internal diameter of 0.8 mm and an external diameter of 1.09 mm. The tip of the capillary was located 2.65 mm below the liquid-air interface that served as a substitute for a large bubble. The bubble was slowly grown until its top was about 0.5 mm below the liquid-air interface. Then, the quasi-static approach to the liquid-air interface was ensured by adding air to the bubble in steps of 150 nL, followed by a waiting period of 30 seconds. The bubble was grown in this way, until the film between bubble and liquid-air interface is about 100 μm. Apparently, from this point the bubble continues to slowly expand without external influence towards the liquid-air interface (due to a slight pressure difference that remains or arises in the syringe, probably because of relaxation motion of the piston). During the approach of the bubble, its top is reflected in the liquid-air interface and the location of the liquid-air interface is estimated by this reflection.

The time point of contact is defined by the frame at which the top of the bubble is observed to just touch its reflection (see figure 2).The coalescence time is measured by counting the video frames from the point of contact to the last frame before coalescence with the liquid-air interface. In cases of rapid coalescence, the two time points were either identical (which estimate coalescence time less than the time interval between frames, ~0.06 seconds) or clearly recognized (figure 2). The standard deviation is presented for each test solution in figure 3 (sometimes too small to be recognized). In cases of slow coalescence, the time point of contact is more ambiguous, hence we independently identified it at least ten times for each video movie. The coalescence times were reproducible with standard deviation of ±0.6 seconds. The total uncertainty in the coalescence times was therefore about 1 sec, which is more than adequate for slow coalescence (>15 min) and for the present purposes. In addition, it should be mentioned that all experiments were performed at a temperature of 296 K and relative humidity of 55%. In all cases the bubble volume at the contact time was similar, as calculated from the shapes of the bubbles (9 ± 0.3 μL).

The experiments were repeated at least 10 times for each solution using three different preparations. The measurements for each test solution were found to be very reproducible, and their averages and standard deviations are presented in figure 3. The approach velocity of the top of the bubble was directly calculated from the video frames preceding the touching of the interface, where the coalescence process/dynamics takes place. It was within the range of 1–10 μm/sec in all experiments, which fits the definition of the quasi-static range[32].

The aqueous solutions were prepared with purified water, obtained by ultrafiltration (Elgar UHQ system) of Reverse Osmosis water. The measured pH is 5.8, due to CO_2 dissolution and speciation in the water. The highest measured conductivity of the purified water, as received from the purification system, was 10 μS m^{-1}, and it changed to at most 20 μS m^{-1} after one day in our system (only some of the pure water experiments were done with day-old water; all other experiments were performed within a short time of getting the purified water). For "CO_2-free" water experiment, the purified water (Reverse Osmosis water) was boiled to release the dissolved carbon dioxide[51]. Then, it was cooled to room temperature and applied to the system under ultra-zero air conditions. Conductivity and pH of the boiled water were 11 ± 5 μS m^{-1} and 6.5 respectively, which corresponds to a negligible CO_2–speciation in the water. Other techniques to get "CO_2-free" system, e.g. nitrogen or noble gas treatment, produced too much artefacts in our system. We repeat this experiment 10 times and found it to be reproducible (±2.5 sec).

The following salts were used: 99.5% analytical sodium chloride (Frutarom chemicals), 99.4% analytical, potassium acetate (Baker chemicals), chemically pure 99.5% potassium chloride (Frutarom chemicals), and 99.99% analytical sodium acetate (Merck chemicals). The acidic solutions used were: 1.000 ± 0.002 M hydrochloric acid, 1.000 ± 0.002 M nitric acid, 1.000 ± 0.002 M acetic acid, and 0.500 ± 0.001 M sulfuric acid, all by Merck chemicals, primary standard solutions. The basic solutions used were: 1.000 ± 0.001 M sodium hydroxide (Merck chemicals, primary standard solution), and 5.0 M ammonium hydroxide (Fluka analytical, Traceable to NIST). To ensure that there were no surface active impurities in the tested solutions, surface tension of purified water and salt solutions (1 M) were measured by the pendant drop method. The results were: 71.5 ± 0.1, 73.8 ± 1.2, 73.4 ± 1.1, 73.7 ± 1.2, 73.1 ± 0.9 mN m^{-1} for purified water, 1 M NaCl, 1 M KCl, 1 M KAc, 1 M NaAc respectively.

The electrolytes were chosen in such a way that all "α,β" classifications are represented: (1) Salts: NaCl (αα), KCl (αα), NaAc (αβ) and KAc (αβ); (2) Acids: HCl (βα), HNO_3 (βα), H_2SO_4 (βα) and HAc (ββ); and (3) Bases: NaOH (αα) and NH_4OH (αα). Electrolytic aqueous solutions were studied over a concentration range of 10^{-6} M to 1 M, prepared by dilutions with purified water. The pH value of each solution was measured before and after the coalescence process (using Combination pH glass Electrode; Hanna Instruments 1043). In most experiments the gas phase was atmospheric air, except for "CO_2-free" experiment in water, for which ultra-zero air (RIVOIRA, $CO_2 < 1$ ppm) was used.

1. Winkel, E. S., Ceccio, S. L., Dowling, D. R. & Perlin, M. Bubble-size distributions produced by wall injection of air into flowing freshwater, saltwater and surfactant solutions. *Exp. Fluids.* **37**, 802–810 (2004).
2. Hofmeier, U., Yaminsky, V. V. & Christenson, H. K. Observations of solute effects on bubble formation. *J. Coll. Interface Sci.* **174**, 199–210 (1995).
3. Lamarre, E. & Melville, W. K. Air entrainment and dissipation in breaking waves. *Nature.* **351**, 469–472 (1991).
4. Deane, G. B. & Stokes, M. D. Scale dependence of bubble creation mechanisms in breaking waves. *Nature.* **418**, 839–844 (2002).
5. Thorpe, A. S. On the clouds of bubbles formed by breaking wind-waves in deep water, and their role in air-sea gas transfer. *Phil. Trans. R. Soc. Lond. A.* **304**, 155–210 (1982).
6. Slauenwhite, D. E. & Johnson, B. D. Bubble shattering: differences in bubble formation in fresh water. *J. Geophys. Res. – Ocean.* **104**, 3265–3275 (1999).

7. Farmer, D. M., Mcneil, C. L. & Johnson, B. D. Evidence for the importance of bubbles in increasing air-sea gas flux. *Nature.* **361**, 620–623 (1993).
8. Linek, V., Benes, P. & Holecek, O. Correlation for volumetric mass transfer coefficient in mechanically agitated aerated vessel for oxygen absorption in aqueous electrolyte solutions. *Biotechnol. Bioeng.* **32**, 482–490 (1988).
9. Tanaka, Y., Kilkuchi, K., Saihara, Y. & Ogumi, Z. Bubble visualization and electrolyte dependency of dissolving hydrogen in electrolyzed water using solid-polymer-electrolyte. *Electrochim. Acta.* **50**, 5229–5236 (2005).
10. Schnurmann, R. The size of gas bubbles in liquids. *Z. Phys. Chem.* **143**, 456–474 (1929).
11. Deschenes, L. A., Barrett, J., Muller, L. J., Fourkas, J. T. & Mohanty, U. Inhibition of bubble coalescence in aqueous solutions. 1. Electrolytes. *J. Phys. Chem. B.* **102**, 5115–5119 (1998).
12. Tse, K., Martin, T., McFarlane, C. M. & Nienow, A. W. Visualization of bubble coalescence in a coalescence cell, a stirred tank and a bubble column. *Chem. Eng. Sci.* **53**, 4031–4036 (1998).
13. Ribeiro, C. P. & Mewes, D. On the effect of liquid temperature upon bubble coalescence. *Chem. Eng. Sci.* **61**, 5704–5716 (2006).
14. Craig, V. S. J., Ninham, B. W. & Pashley, R. M. The effect of electrolytes on bubble coalescence in water. *J. Phys. Chem.* **97**, 10192–10197 (1993).
15. Henry, C. L., Dalton, C. N., Scruton, L. & Craig, V. S. J. Ion-specific coalescence of bubbles in mixed electrolyte solutions. *J. Phys. Chem. C.* **111**, 1015–1023 (2007).
16. Prince, M. J. & Blanch, H. W. Bubble coalescence and break-up in air-sparged bubble columns. *AlChE J.* **36**, 1425–1429 (1990).
17. Marrucci, G. & Nicodemo, L. Coalescence of gas bubbles in aqueous solutions of inorganic electrolytes. *Chem.Eng.Sci.* **22**, 1257–1265 (1967).
18. Keitel, G. & Onken, U. Inhibition of bubble coalescence by solutes in air/water dispersions. *Chem. Eng. Sci.* **37**, 1635–1638 (1982).
19. Cain, F. W. & Lee, J. C. A technique for studying the drainage and rupture of unstable liquid films formed between two captive bubbles: measurements on KCI solutions. *J. Coll. Interface Sci.* **106**, 70–85 (1985).
20. Nguyen, P. T., Hampton, M. A., Nguyen, A. V. & Birkett, G. R. The influence of gas velocity, salt type and concentration on transition concentration for bubble coalescence inhibition and gas holdup. *Chem. Eng. Res. Des.* **90**, 33–39 (2012).
21. Christenson, H. K., Bowen, R. E., Carlton, J. A., Denne, J. R. M. & Lu, Y. Electrolytes that show a transition to bubble coalescence inhibition at high concentrations. *J. Phys. Chem. C.* **112**, 794–796 (2008).
22. Sagert, N. H. & Quinn, M. J. The coalescence of gas bubbles in dilute aqueous solutions. *Chem. Eng. Sci.* **33**, 1087–1095 (1978).
23. Bournival, G., Pugh, R. J. & Ata, S. Examination of NaCl and MIBC as bubble coalescence inhibitor in relation to froth flotation. *Mineral Eng.* **25**, 47–53 (2012).
24. Tsang, Y. H., Koh, Y. H. & Koch, D. L. Bubble-size dependence of the critical electrolyte concentration for inhibition of coalescence. *J. Coll. Interface Sci.* **275**, 290–297 (2004).
25. Aguilera, M. E., Ojeda, A., Rondon, C. & de Ramos, A. L. Effect of Electrolytes on Bubble Coalescence in Columns Observed with Visualization Techniques. *Ann. N.Y. Acad. Sci.* **972**, 242–246 (2002).
26. Lessard, R. R. & Zieminski, S. A. Bubble coalescence and gas transfer in aqueous electrolytic solutions. *Ind. Eng. Chem. Fundam.* **10**, 260–269 (1971).
27. Sato, A., Aoki, M. & Watanabe, M. Single Rising Bubble Motion in Aqueous Solution of Electrolyte. *J. of Fluid Sci. Tech.* **5**, 14–25 (2010).
28. Ghosh, P. Coalescence of air bubbles at air-water interface. *Chem. Eng. Research and Design.* **82**, 849–854 (2004).
29. Kirkpatrick, R. D. & Lockett, M. J. The influence of approach velocity on bubble coalescence. *Chem. Eng. Sci.* **29**, 2363–2373 (1974).
30. Castillo, L. A. D., Ohnishi, S. & Horn, R. G. Inhibition of bubble coalescence: Effects of salt concentration and speed of approach. *J. Coll. Interface Sci.* **356**, 316–324 (2011).
31. Karakashev, S. I., Nguyen, P. T., Tsekov, R., Hampton, M. A. & Nguyen, A. V. Anomalous ion effects on rupture and lifetime of aqueous foam films formed from monovalent salt solutions up to saturation concentration. *Langmuir.* **24**, 11587–11591 (2008).
32. Yaminsky, V. V., Ohnishi, S., Vogler, E. A. & Horn, R. G. Stability of aqueous films between bubbles. Part 1. The effect of speed on bubble coalescence in purified water and simple electrolyte solutions. *Langmuir.* **26**, 8061–8074 (2010).
33. Yaminsky, V. V., Ohnishi, S., Vogler, E. A. & Horn, R. G. Stability of aqueous films between bubbles. Part 2. effects of trace impurities and evaporation. *Langmuir.* **26**, 8075–8080 (2010).
34. Tabor, R. F., Chan, D. Y. C., Grieser, F. & Dagastine, R. R. Anomalous stability of carbon dioxide in pH-controlled bubble coalescence. *Angew. Chem. Int. Ed.* **50**, 3454–3456 (2011).
35. Tabor, R. F. *et al.* Homo and hetero-interactions between air bubbles and oil droplets measured by atomic force microscopy. *Soft Matter.* **7**, 8977–8983 (2011).
36. Browne, C. *et al.* Bubble coalescence during acoustic cavitation in aqueous electrolyte solutions. *Langmuir.* **27**, 12025–12032 (2011).
37. Marcelja, S. Selective coalescence of bubbles in simple electrolytes. *J. Phys. Chem. B.* **110**, 13062–13067 (2006).
38. Exerowa, D. & Kruglyakov, P. M. [Volume 5: Theory, Experiment, Application]. *Foam and Foam Films*. (Elsevier Press, Amsterdam, 1998).
39. Maheshwari, R., Sreeram, K. J. & Dhathathreyan, A. Surface energy of aqueous solutions of Hofmeister electrolytes at air/liquid and solid/liquid interface. *Chem. Phys. Lett.* **375**, 157–161 (2003).
40. Li, Z. & Lu, B. C. Surface tension of aqueous electrolyte solutions at high concentrations representation and prediction. *Chem. Eng. Sci.* **56**, 2879–2888 (2001).
41. Stoyanov, S. D. & Benkov, N. D. Role of surface diffusion for the drainage and hydrodynamic stability of thin liquid films. *Langmuir.* **17**, 1150–1156 (2001).
42. Jungwirth, P. & Tobias, D. J. Specific Ion Effects at the Air/Water Interface. *Chem. Rev.* **106**, 1259–1281 (2006).
43. Pegram, L. M. & Record, M. T. Partitioning of atmospherically relevant ions between bulk water and the watervapor interface. *PNAS.* **103**, 14278–14281 (2006).
44. Craig, V. S. J. Do hydration forces play a role in thin film drainage and rupture observed in electrolyte solutions? *Curr. Opin. Colloid Interface Sci.* **16**, 597–600 (2011).
45. Weissenborn, P. K. & Pugh, R. J. Surface tension of aqueous solutions of electrolytes: relationship with ion hydration, oxygen solubility, and bubble coalescence. *J. Coll. Interface. Sci.* **184**, 550–563 (1996).
46. Miklavcic, S. J. Deformation of fluid interfaces under double-layer forces stabilizes bubble dispersions. *Phys. Rev. E.* **54**, 6551–6556 (1996).
47. Craig, V. S. J., Ninham, B. W. & Pashley, R. M. Comment on Deformation of fluid interfaces under double-layer forces stabilizes bubble dispersions. *Phys. Rev. E.* **57**, 7362–7363(1998).
48. Miklavcic, S. J. Reply to Comment on Deformation of fluid interfaces under double-layer forces stabilizes bubble dispersions. *Phys. Rev. E.* **57**, 7364 (1998).
49. Henry, C. L., Parkinson, L., Ralston, J. R. & Craig, V. S. J. A mobile gas-water interface in electrolyte solutions. *J. Phys. Chem. C.* **112**, 15094–15097 (2008).
50. Seinfeld, J. H. & Pandis, S. N. *Atmospheric Chemistry and Physics: From Air Pollution to Climate Change* (John Wiley & Sons, New York, 2006).
51. Crovetto, R. Evaluation of solubility data of the system CO_2-H_2O from 273 K to the critical point of water. *J. Phys. Chem. Ref. Data.* **20**, 575–589 (1991).
52. Takahashi, M. Zeta-potential of microbubbles in aqueous solutions: electrical properties of the gas-water interface. *Phys. Chem. B.* **109**, 21858–21864 (2005).
53. Cho, S. H., Kim, J. Y., Chun, J. H. & Kim, J. D. Ultrasonic formation of nanobubbles and their zeta-potentials in aqueous electrolyte and surfactant solutions. *Colloids and Surfaces A: Physicochem. Eng. Aspects.* **269**, 28–34 (2005).
54. Najafi, A. S., Drelich, J., Yeung, A., Xu, Z. & Masliyah, J. A novel method of measuring electrophoretic mobility of gas bubbles. *J. Coll. and Interface Sci.* **308**, 344–350 (2007).
55. Yang, C., Dabros, T., Li, D., Czarnecki, J. & Masliyah, J. H. Measurement of the Zeta Potential of Gas Bubbles in Aqueous Solutions by Microelectrophoresis Method. *J. Coll. and Interface Sci.* **243**, 128–135 (2001).
56. Beattie, J. K. & Djerdjev, A. M. The Pristine Oil/Water Interface: Surfactant-Free Hydroxide-Charged Emulsions. *Angew. Chem. Int. Ed.* **43**, 3568–3571 (2004).
57. Beattie, J. K., Djerdjev, A. M. & Warr, G. G. The surface of neat water is basic. *Faraday Discuss.* **141**, 31–39 (2008).
58. Creux, P., Lachaise, J., Graciaa, A., Beattie, J. K. & Djerdjev, A. Strong Specific Hydroxide Ion Binding at the Pristine Oil/Water and Air/Water Interfaces. *J. Phys. Chem. B.* **113**, 14146–14150 (2009).
59. Kruyt, H. R., Jonker, H. & Overbeek, T. G. [Volume 1: Irreversible Systems]. *Colloid Science*. [Kruyt, H. R. (ed.)], (Elsevier Publishing Company, Amsterdam-Houston-New York-London, 1952).
60. Israelachvili, J. *Intermolecular and Surface Forces* (Academic Press, London, 1992).

Author contributions

A.M. and Y.K. contributed equally to this work.

Additional information

Competing financial interests: The authors declare no competing financial interests.

How to cite this article: Katsir, Y. & Marmur, A. Rate of Bubble Coalescence following Quasi-Static Approach: Screening and Neutralization of the Electric Double Layer. *Sci. Rep.* **4**, 4266; DOI:10.1038/srep04266 (2014).